Ocean Dynamics (2007) 57: 135–149
DOI 10.1007/s10236-006-0095-9

Hans van Haren

Echo intensity data as a directional antenna for observing processes above sloping ocean bottoms

Received: 12 April 2006 / Accepted: 13 November 2006 / Published online: 12 January 2007

Abstract Relative 'echo intensity' data (dI) from a bottom-mounted four-beam 300 kHz acoustic Doppler current profiler (ADCP) are used to infer propagation of vigorous processes above a continental slope. The 3- to 60-m horizontal beam spread and the 2-Hz sampling allow the distinction of different arrival times t_i, i=1,..., 4, at different distances in the acoustic beams from sharp changes in dI-content associated with frontal non-linear and turbulent bores or 'waves'. The changes in dI are partially due to variations in amounts of resuspended material carried by the near-bottom turbulence and partially due to the fast variations in density stratification ('stratified turbulence'), as inferred from 1-Hz sampled thermistor string data above the ADCP. Such bores are observed to pass the mooring up to 80 m above the bottom, having typical propagation speeds c=0.15–0.5 m s^{-1}, as determined from $dI(t_i)$. Particle speeds in the immediate environment of a bore amount to $|\mathbf{u}|_{env}=c\pm0.05$ m s^{-1}, the equality being a necessary condition for kinematic instability, whilst the maximum particle speeds amount $|\mathbf{u}|_{max}$=1.2–2c. The dI-determined directions of up-, down- and alongslope processes are all to within ±10° of the ADCP's beam-spread averaged current (particle velocity) data.

Keywords ADCP echo intensity observations · Near-bottom processes · Continental slope · Propagation and particle speeds · Bay of Biscay

1 Introduction

The thermal unrest in the density stratified ocean is dramatically visualized near its edges: above sloping topography. Although debate is ongoing (Armi 1978; Garrett 1990; Lamb et al. 2005) whether mixing above slopes is actually efficient enough to account for Munk's (1966) proposal that turbulent diapycnal mixing balances the ocean interior's heat transport, it is commonly accepted that vigorous processes do occur above sloping bottoms. The reason for such vigour is simple. Although above any bottom frictional turbulent boundary layers can develop, only above a sloping bottom the stable stacked density surfaces are, on average, under a non-zero angle to the bottom so that gravitational processes (Garrett 1990; MacCready and Rhines 1993), internal wave critical reflection (Dauxois et al. 2004) and internal wave breaking (Thorpe 1975; Ivey and Nokes 1989) can occur.

Furthermore, recent modelling (Vlasenko and Hutter 2002; Lamb et al. 2005) and observations (Klymak and Moum 2003; Hosegood et al. 2004) have shown that interior relaxation of a sloping density surface may initiate a steep frontal bore with trailing waves that may propagate up the slope whilst passing moored instrumentation within minutes. As such a 'solibore' can dominate sediment resuspension processes (Hosegood et al. 2004), interest has grown in the establishment of its precise development, including the direction of propagation in relation to the direction of the bottom slope. Sparse observational examples suggest that most turbulent resuspension occurs when a solibore moves strictly perpendicular up the slope, when particle speed $|\mathbf{u}|$ exceeds phase propagation speed c, $|\mathbf{u}|/c > 1$, whereas a train of not necessarily turbulent solitary waves is expected when the front moves obliquely across the slope (Hosegood and van Haren 2004).

Therefore, for further understanding the importance of various near-bottom resuspension processes, it is imperative to know the propagation speed and direction of the different phenomena with respect to the local orientation of the slope. This implies first a sufficiently high sampling rate O(1 Hz) to capture processes that pass within minutes. Second, a detailed sampling of currents, stratification and suspended material is required in the vertical to resolve variations O(1–10 m). Naturally, a three (or four)-beam acoustic Doppler current profiler (ADCP) meets most of the requirements, as it measures all three Cartesian (x, y, z)

Responsible editor: Jin-Song von Storch

H. van Haren (✉)
Royal Netherlands Institute for Sea Research (NIOZ),
P.O. Box 59, 1790 AB Den Burg, The Netherlands
e-mail: hansvh@nioz.nl
Tel.: +31-222-369451
Fax: +31-222-319674

current components (along-slope u, cross-slope v, bottom-normal w) and the back-scattered amplitude ('echo intensity' I) as a function of distance from the instrument.

As a small disadvantage, one needs to establish the relationship between measured echo intensity and suspended matter content and, perhaps, amount of stratification. As a further disadvantage, the ADCP's originally measured 'Doppler-shifted' beam-velocities b_i, i=1, 2, 3(, 4), are a linear combination of (u, v, w), because the 3(4) beams are slanted at a typical angle θ=20–30° to the vertical. As a result, particle velocities (currents) are averages over the horizontal beam spread, and direct evidence of (phase) propagation of a front or wave can, in principle, only be obtained by deploying several ADCP's close together. Even then, the resolved (horizontal) length scale is still larger than the beam spread and determined by the distance between moorings. If the near-bottom process is exclusively characterized by w or u, v, one could transfer these Cartesian current data back to the original b_i to obtain a much higher spatial resolution as the spherical spreading of each beam is about 1.5°. However, the use of b_i is only useful when single ping (single acoustic transmission) data are stored, as ensemble averaging of more than one ping data is performed in Cartesian coordinates only. In general, the use of b_i is not an option, also because current characteristics of the phenomena are not precisely known a priori and because current estimates in vigorous environments are often flagged 'bad' using the general criteria that are partially based on 'reasonable homogeneity' over the beam spread.

In this paper, an alternative manner of detecting near-bottom processes is explored, as an ADCP does provide I data directly within each beam. As I data are a measure of variations in acoustic backscatter, it is of lesser concern here whether they are attributable to actual suspended material or, for example, to immaterial stratified turbulence (Thorpe and Brubaker 1983; Lhermitte and Lemmin 1990; Ross and Lueck 2003). Any propagating means that carries a slightly different backscatter with respect to its environment passed each of the slanted beams evidences a vigorous process. As will be demonstrated, the variations in I between the different beams, here from a steep slope in the deep Bay of Biscay, are not attributable to flow disturbance by the mooring as reported for shallow turbid waters by Fuda et al. (2006). They found I increases in beam(s) on one side corresponding with I decreases in the opposing beam(s) that were strongly associated with flow obstruction due to their large bottomlander.

2 Materials and methods

Details of investigation site and instrumentation are given in Fig. 1 and Table 1. At ~1,450 m of the continental slope in the Bay of Biscay, a bottomlander was deployed holding an upward-looking 300-kHz RDI Sentinel ADCP with 2-GB memory and a single-point 2-MHz Nortek AquaDopp 3-D acoustic current meter. Attached to the centre of the bottomlander was an 80-m long mooring line, mainly

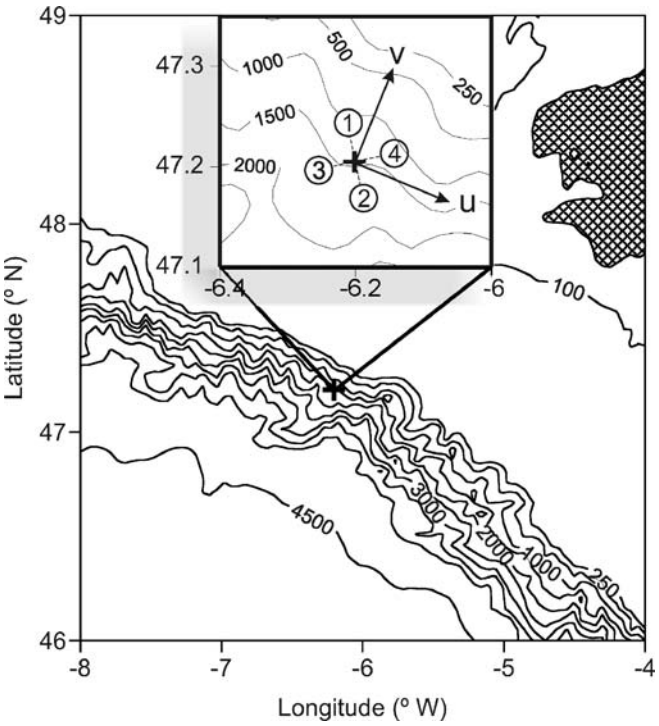

Fig. 1 Bay of Biscay continental slope southwest of Brittany (F; upper-right corner), with horizontal current axes and orientation of the four ADCP beams (not to scale) around mooring position + in *inset*. Water depths in metres

holding temperature sensors and another AquaDopp, below a low-drag elliptical sub-surface buoy of 200-kg net buoyancy. All instruments sampled at 1 Hz, except for the ADCP that sampled single ping data at 2 Hz.

The four-beam ADCP was mounted at the top of the bottomlander, as far as possible from the thermistor string attachment, with its beams pointing under ~45°, that is maximal away from the string. The lander itself is a 3×2×1.5 m open aluminium frame, holding two layers of four glass-sphere buoyancy elements on both long sides. These elements somewhat obstruct the flow locally, but they do not seem to affect flow higher than z~3 m above the bottom.

As an independent measure for (rapid) variations in stratification, first differences dT/dz of temperature (T) data are used from the τ<0.5 s response time, 0.001 K accurate

Table 1 Mooring details

Property	Value
Bottom slope estimate	β=4.6±0.5°
Deployment	23/04/2005 02 UTC
Recovery	25/04/2005 08 UTC
Nortek AquaDopp	z=1.75, 68 m; rate 1 s
NIOZ-2 thermistor string	z=2.1–65.6 m every 0.5 m; rate 1 s
300-kHz RDI ADCP	z=6.6–85.6 m every 1.0 m; rate 0.5 s

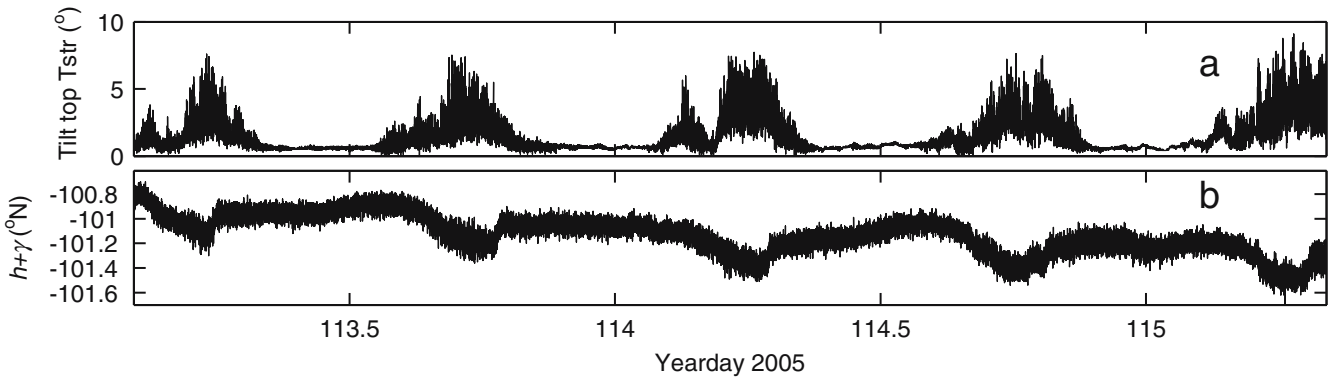

Fig. 2 **a** Tilt at upper current meter (z=68 m) just below top buoy. **b** ADCP's heading h, corrected for local magnetic declination γ

NIOZ-2 thermistor string that carries 128 sensors at 0.5 m intervals (van Haren et al. 2005). Unfortunately, sealing problems caused failure of some 35 sensors. The position of the thermistor string due to non-zero drag in the dynamic environment is inferred from pressure (P) and tilt (Ti) information at the AquaDopp above it. A typical 5° tilt (Fig. 2a) implies an average horizontal sway amplitude of 2.8 m and a vertical one of 0.12 m.

The Bay of Biscay continental slope is very rugged, with many small-scale topographic features (Fig. 1). The precise local bottom slope is difficult to determine because it depends on the typical length scales of the phenomenon to be studied. If we estimate turbulent overturns and small-scale topography to have length scales O(10–100 m) here and because both the ship's echo sounder and the ETOPO-2 map have resolution equal to or larger than this, the result is a misfit of some 150–200 m in depth determination. Over a larger 5′ (~9 km) grid, the local bottom slope $\beta \approx 4$–5°, which compares well with the ADCP tilt data.

This slope is oriented $\nu = 22.5 \pm 1.5$°N from North (ν-current directed upslope). As the magnetic declination ($\gamma = -4.0$°W) corrected ADCP's mean heading $h + \gamma = -101.13 \pm 0.15$°N (Fig. 2b), the beam orientation is such that beam 2 is located most downslope (Fig. 1). It is noted that the ADCP's heading is not constant with time, probably because the bottomlander is moved slightly by occasionally strong currents up to 0.5 m s^{-1} near the bottom.

Although the ADCP was not gimballed in the bottom-lander, the bottom slope did not pose a problem on the data quality (because $\beta << \theta = 20$°). Data quality was somewhat affected by sparse hard (side-lobe) reflections off thermistor string sensors, clearly visible in the records. It is noted that the slightly swaying thermistor string remains always within the four ADCP-beams for z>6 m, as upper current meter's tilt + $\beta < \theta$. ADCP data quality is more often affected by the single-ping sampling in this deep and turbulent environment. Although this 'undersampling' affected beam-spread averaged current estimates of which quite a few were flagged 'bad', the I were never flagged 'bad' over the entire range of 80 m throughout the measurement period (see below). In contrast, AquaDopp's 'single-point' current estimates were less affected by the environmental conditions, as they were generally labeled 'good'.

2.1 Determining relative echo intensity in practice

After transferring the ADCP's raw $I(z)$ from units 'counts' to 'dB' by multiplication with a factor of 0.45, these data do contain large uninteresting signal due to sound absorption in the water and beam spreading (RDI 1996),

$$I = S + B - 20\log(R) - 2\alpha R + C, \ \ in\ dB \qquad (1)$$

where S denotes the source level that can vary for every single transducer, and $B(z)$ is the water-mass volume backscatter strength: the quantity of interest here. The radial distance from the transducer to a depth cell (measurement volume) is given by $R = (z - z_A)/\cos\theta$, z_A the depth of the ADCP, whereas α denotes the absorption coefficient and C a constant. The 20log$R$-term accounts for spherical spreading of each beam. For a 300-kHz system at 4°C, 35 ppt salinity and atmospheric pressure, $0.062 \le \alpha \le 0.084$ dB m^{-1} (RDI 1996), with the uncertainty mainly due

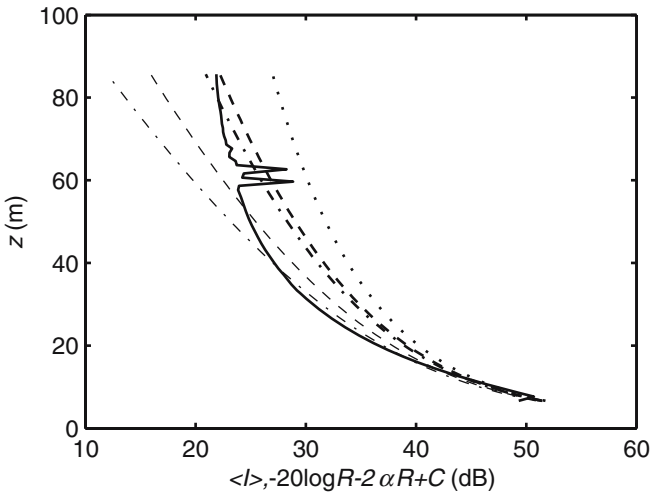

Fig. 3 Time mean $<I>$ observed using beam 1 (*solid line*) with first side-lobe reflections at thermistor string recorder and top buoy visible near z=60 m. The heavy dash-dot and dashed lines indicate spherical beam spread and attenuation terms 20log$R - \alpha R$ + arbitrary C, using α extremes of (2) following Urick (1975), whereas the *thin ones* are computed using ~double these values for α (RDI 1996, see text). The *dotted line* is for 20log$R$ (α=0)

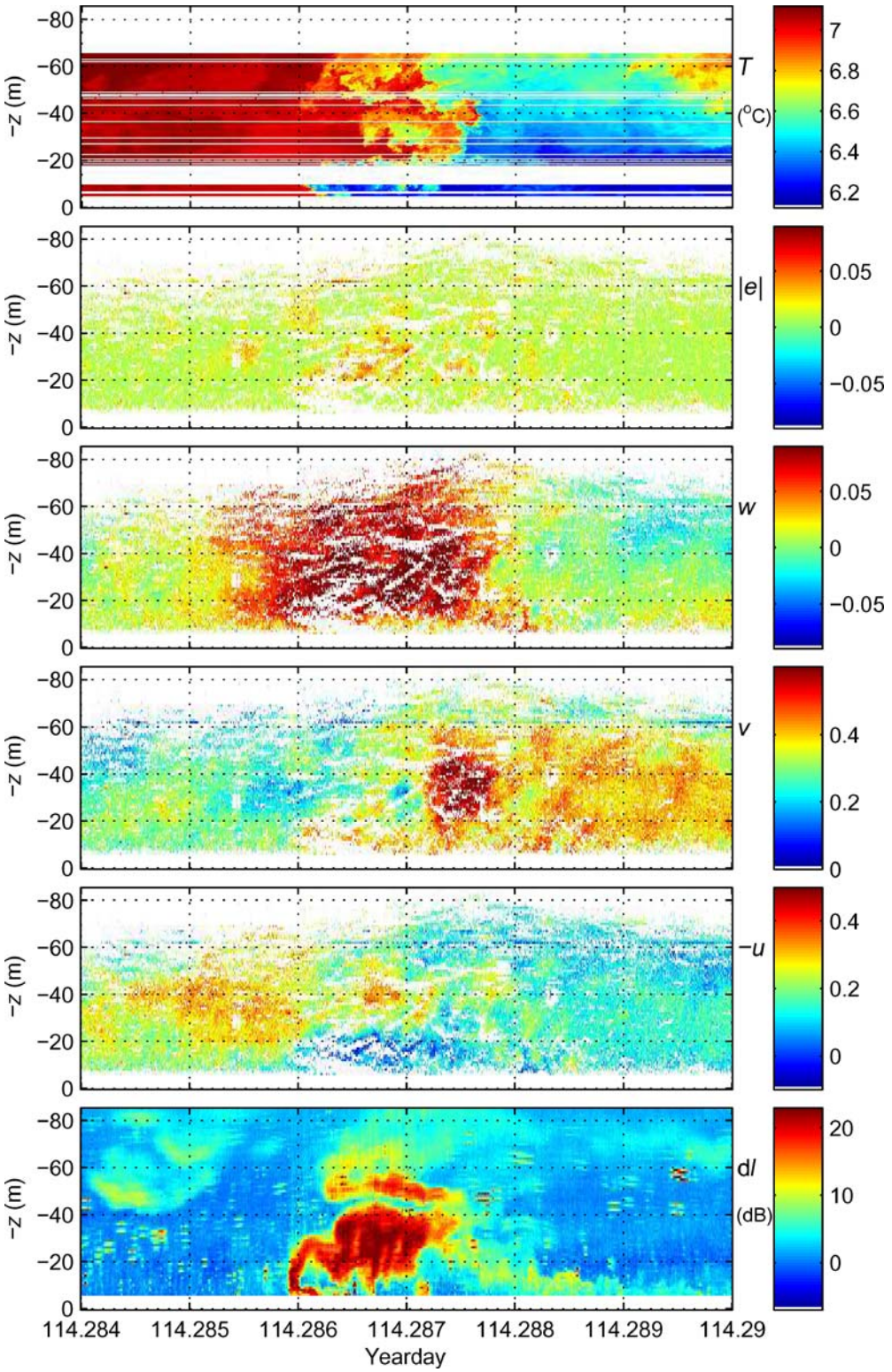

Fig. 4 Short period (7 min) example of thermistor string T and ADCP data during the passage of a near-bottom front. All current components including error velocity e defined in (6) are in metres per second. The w and $|e|$ have the same range of values for proper comparison. The *white spots and bands* indicate 'bad' or 'no' data. Bands of bad ADCP current data seem to align with layers of large dI and T variations. The dI are from beam 3

to lack of knowledge on true absorption. However, Urick (1975) provides a formula that yields half these values, or more precisely, Urick gives values for 2α when used in (1),

$$\alpha = 4.0 \pm 0.2 \cdot 10^{-7}\sigma_t^2\left(1 - 6.54 \cdot 10^{-5}P\right), \quad in\, dB\, m^{-1} \tag{2}$$

also for non-atmospheric pressures P in dbar, with transmit frequency σ_t in kHz.

The interesting signal B can be computed from (1) provided the absorption is precisely known, including temperature variations throughout time and depth. Follow-

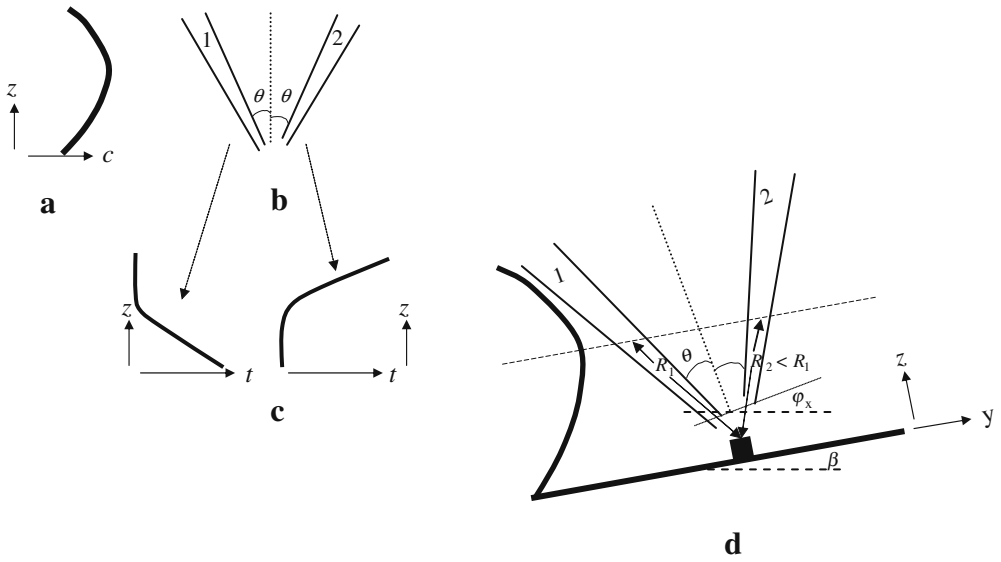

Fig. 5 Sketch of possible registration of a curved ('backwards breaking') front moving at speed c (**a**), passed an ADCP's beams 1, 2 (**b**), resulting in different z, t registrations of dI (*black* high value, *white* low value; **c**). Sketch defining the angles of a tilted pair of beams on a sloping bottom (*straight heavy solid line*) and showing the different radial distances R_1, R_2 to the ADCP at which a front that propagates at a fixed height above the bottom is measured in opposing beams (**d**)

ing the above, however, uncertainty exists in the definition of sound energy level, being a relative measure expressed in dB units. Furthermore, in practice, the given uncertainty in α is usually far too large for a proper measure of determining actual B (Fig. 3): none of the curves computed using α estimates approaches the curvature of observed mean $<I>$ (to within arbitrary constant). Urick's values correspond with begin- and endpoints of the ADCP's range, whereas RDI's values predict a reasonable curvature but for the first 20 m of the range only. The misfits of the estimates amount to ±2 dB (1 std). As a result, it is more feasible to compute per z, per averaging period $<>$, a *relative* echo intensity as a measure for B,

$$dI = I - < I > \approx B, \quad in\, dB \tag{3}$$

due to the unknown sound source level of the individual beams and due to the imprecise knowledge of the sound attenuation through the varying environment. It is noted that the average misfit in mean curves (Fig. 3) is one order of magnitude smaller than the variations induced by phenomena to be studied here (Section 3).

2.2 Determining speed, direction and shape of fronts and waves using dI data

The dI are expected to vary with passages of waves or turbulent bores that carry either large suspended material loads or actively deformed stratification that markedly differ from their environment, see the example in (Fig. 4). Judging from the arrival times t_i at a particular z of a variation in $dI(t_i)$ at the four beams i=1,..., 4, propagation speed (c) and direction angle (d), with respect to upslope direction, of a passing phenomenon can be defined as,

$$\begin{aligned} c &= 2z \cdot \tan\theta \Big/ \left[(t_3 - t_4)^2 + (t_2 - t_1)^2 \right]^{1/2} \\ d &= \arctan\left[(t_1 - t_2) / (t_3 - t_4) \right] + h + \gamma - \nu. \end{aligned} \tag{4}$$

As a complicating factor, the shape of the front may vary during its passage and with distance from the ADCP (bottom). Due to the beam slant to the vertical and the 90° varying beam directions in the horizontal, a passing front will show up differently in the $dI(z, t)$ data from forward and backward slanted beams (Fig. 5), even without changes in frontal structure during the passage. As a result, not just different arrival times at a particular z but also their shape variation in z, t can be used to distinguish the passage of a disturbance. This is straightforward on a flat bottom (Fig. 5a–c), but it needs a correction for bottom slope and local tilt of the ADCP, as a function of propagation direction of the phenomenon observed (Fig. 5d). This is because the internal transformation to Cartesian coordinates, including vertical bins, for ADCP current data is not performed for echo intensity data, as can be verified by comparing strong reflectance at a flat level (e.g. the sea surface) from a beam pair of a tilted instrument (van Haren 2001). The reason why this transformation is not performed automatically in RDI-ADCP's is unknown, but it can be corrected.

With reference to Fig. 5d, if we assume that above a bottom of slope β, physical processes occur in a tilted, bottom–normal coordinate system, an ADCP beam pair tilted at angle φ_x will observe a strictly up- or downslope moving phenomenon not at depths z but at levels $z \cdot \cos(\theta \pm (\varphi_x - \beta)) / \cos(\theta)$ that are either too low (+, backward slanting beam) or too high (−, forward

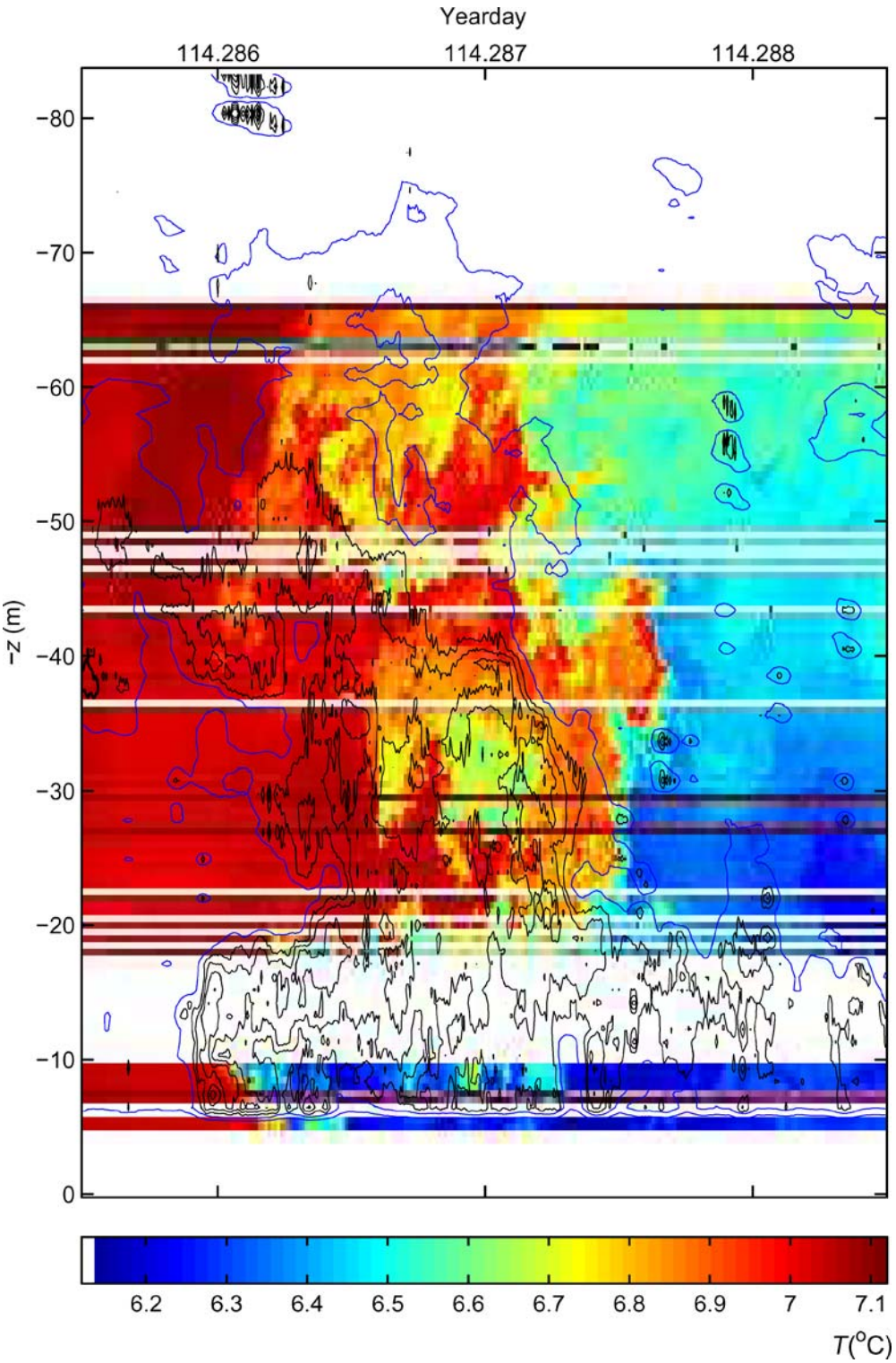

Fig. 6 Detailed comparison between $T(z)$ and $dI_2(z_c)$ during 4 min around passage of the strongest front from Fig. 4. *dI* Contours are for raw 2-Hz data at 10, 15, 20 and 25 dB (*black lines*) and for 5-s smoothed data at 0, 5 dB (*blue*). The contours near z=6.5 m are artificial, bordering ADCP's first depth cell

slanting beam). When the normals to the planes of angles β and φ_x are not in the same plane, depth levels for each beam need a further correction as a function of the (usually unknown) propagation direction ψ, with respect to upslope directions, of the phenomenon to be observed. The entire z correction then reads,

$$\begin{aligned} z_c &= z \cdot \cos\theta / \cos\left(\theta - \varphi_x + \arcsin\left(\sin\beta\cos\psi\right)\right), \quad \text{beam slanted downslope} \\ z_c &= z \cdot \cos\theta / \cos\left(\theta + \varphi_x - \arcsin\left(\sin\beta\cos\psi\right)\right), \quad \text{beam slanted upslope,} \end{aligned} \tag{5}$$

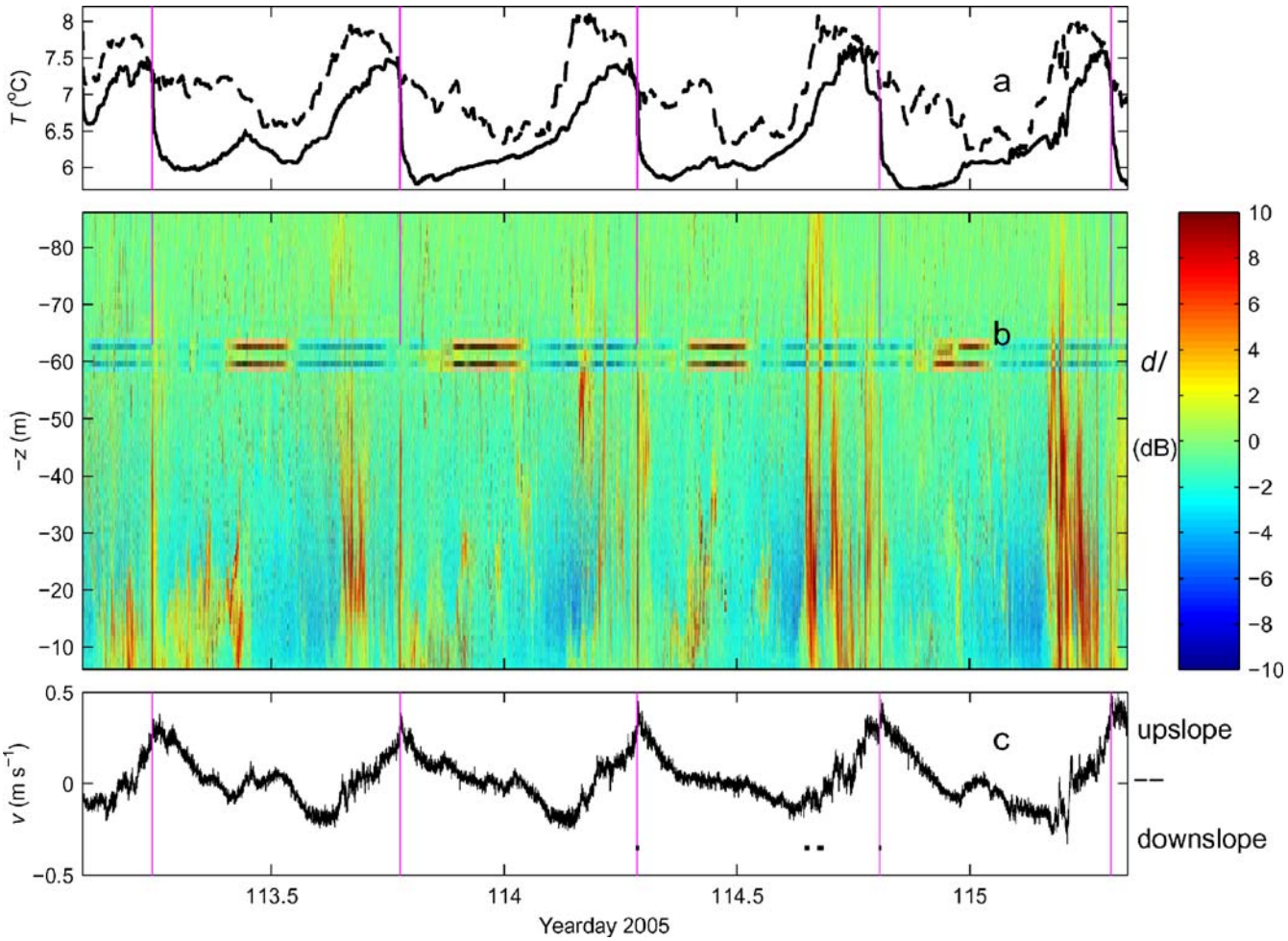

Fig. 7 Total time series of **a** temperature measured at z=1.7 (*solid*) and 68 m (*dashed*), **b** relative echo intensity of ADCP's beam 1, between 6.6–85.6 m, **c** cross-slope current measured at 1.7 m. The *purple vertical lines* indicate the passage of steepest temperature drop observed within each tidal period at 1.7 m. The *four black ticks* at the level of v=−0.35 m s^{-1} indicate the periods of Figs. 8 and 9, 12 and 13, 14 and 15, and 10 and 11 (*left-right*)

assuming a slope that is uniform over the length scale of interest.

Application of (5) yields a reasonably good comparison between variations observed at particular depths in dI_2 and in independently measured T (Fig. 6). The form of the front, layers of enhanced stratification and spots of overturning are recognizable in both, with especially good correspondence in the near-bottom front (z<20 m), in the core near 30 m, day 114.287 and in the ~20 s period wave-like motions near 10 m after the passage of the near-bottom front. Some discrepancies remain: the timing of especially the upper front (z>20 m) is different, which is a major subject of discussion in Section 3, with progressively more advanced arrival in dI_2 for larger z_c in this example, and T data show more coherent detailed structures, even in overturning layers. The mismatch in precise location of high gradients in T and dI is partially due to variation in developing turbulence with time, as sampling in beam 2 and the thermistor string are not exactly at the same position, besides the different quantities measured. The lesser detail in dI is due to more smoothed sampling by the ADCP compared to the thermistor string, which even more affects the ADCP's current measurements.

2.3 Measuring u, v, w of a front using ADCP

The passage of, e.g., a frontal bore has a somewhat blurred shape in u, v, w when measured in z, t using an ADCP (Fig. 4). In this example, fine details such as the sharpness of the front (clearly visible in T and dI) and stratified layering (in dI and best in T, also after the front passage) are partially visible in u (becoming near-zero after the frontal passage), v (strong increase upslope) and w (large increase smeared over 2 min in t and with a smaller-scale enhancement superposed so that total w>0.1 m s^{-1}; note the downwelling after day 114.289 for z>40 m). These somewhat blurred current observations are partially due to beam smearing in the vertical, as the transmission length is 3.9 m yielding half-independent vertical scales of ~2 m,

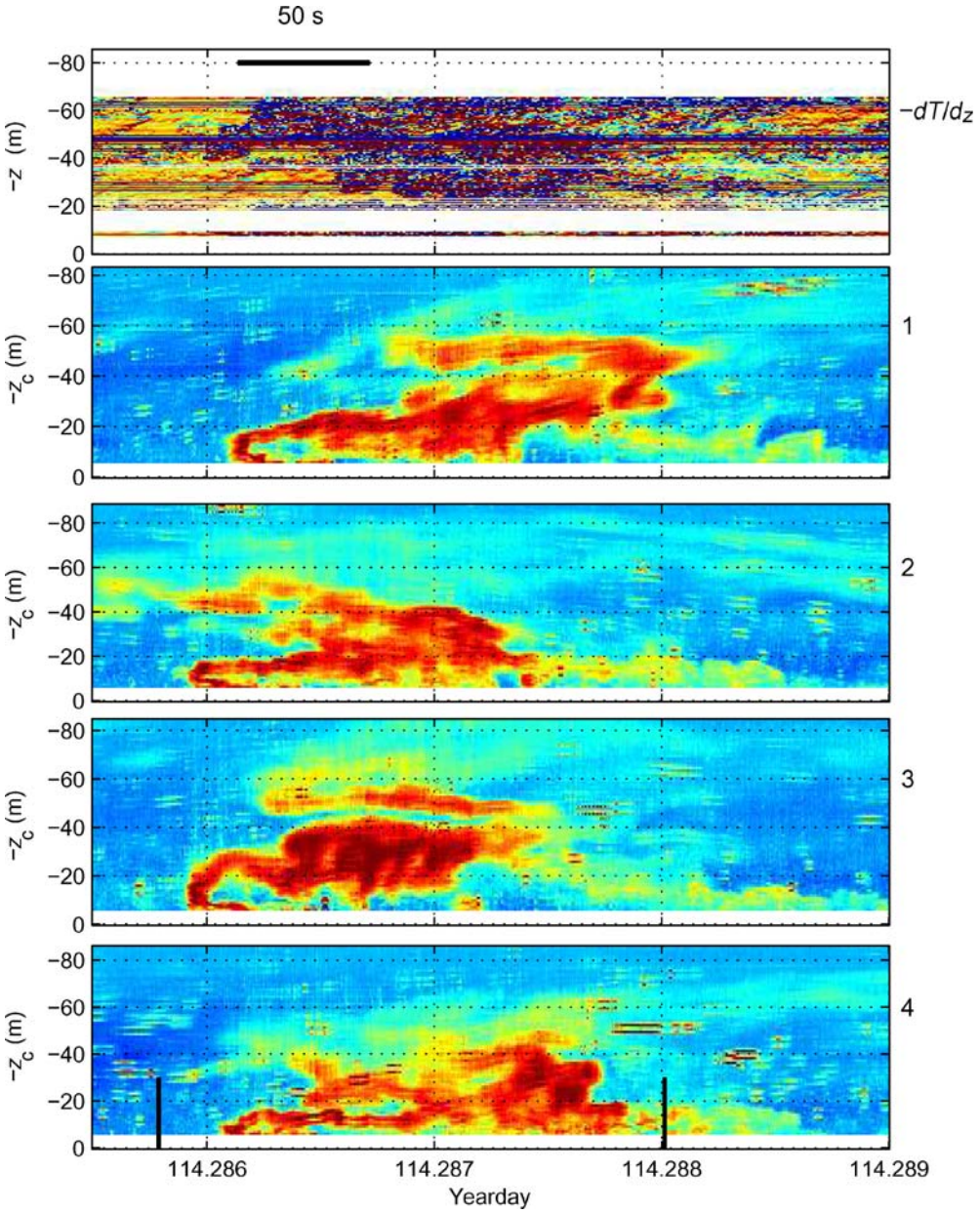

Fig. 8 Temperature gradient (*upper panel*) and relative echo intensity observed at all four beams (indicated 1,..., 4) during the passage of the strongest front. The colour coding for *dI* relative to the mean over the 5-min period is between [−7, 23] dB for (*dark-blue*,..., *dark-red*). The same colours indicate for $-dT/dz$ the range [−0.04, 0.02]°C m^{-1}, with *yellow* at 0, *green-blue* indicating stable stratification and *orange-red* instability. The *vertical bars* in the lowest panel indicate the borders of the period from which current vectors are plotted in Fig. 9

also causing some smearing in *dI*, as well as in the horizontal by the beam spread (not affecting *dI*). Horizontal current inhomogeneity over the beam spread shows up in *w* and, for a four-beam ADCP, equally in magnitude for 'error velocity' *e*, which reads, properly scaled (van Haren et al. 1994),

$$w = w_{true} + (u_1 - u_2 + v_3 - v_4)\tan\theta/4,$$
$$e = -(w_1 + w_2 - w_3 - w_4)/4 - (u_1 - u_2 + v_3 - v_4)\tan\theta/4, \quad (6)$$

provided all four beams deliver 'good' data. Clearly in Fig. 4, most of observed $w \approx w_{true}$ because $|e| << |w|$, except during small periods in the core of the frontal passage that are associated with the aforementioned details, which are thus not well-represented in *w* (and also in *u*, *v*).

3 Observations

The 2.5 days records of current, temperature and echo intensity demonstrate a strong tidal variation with time, which, however, is not purely sinusoidal but rather non-linear with slow variations followed by sudden large changes (Fig. 7). The passage of steepest near-bottom front per tidal period is directly visible in temperature (Fig. 7a) and associated maximum peak in upslope current (Fig. 7c) but also, with difficulty, in *dI* (Fig. 7b): the very thin, dark-red lines are not the purple indicator lines (that are drawn only between 63–86 m in the middle panel) but actual large increases in *dI*. These extremely short-duration frontal passages extending between lowest observational level of z=6 m up to ~60 m are known as solibores or upslope propagating fronts (Hosegood et al. 2004). In addition to these local 'spikes' in *dI* are relatively large periods of

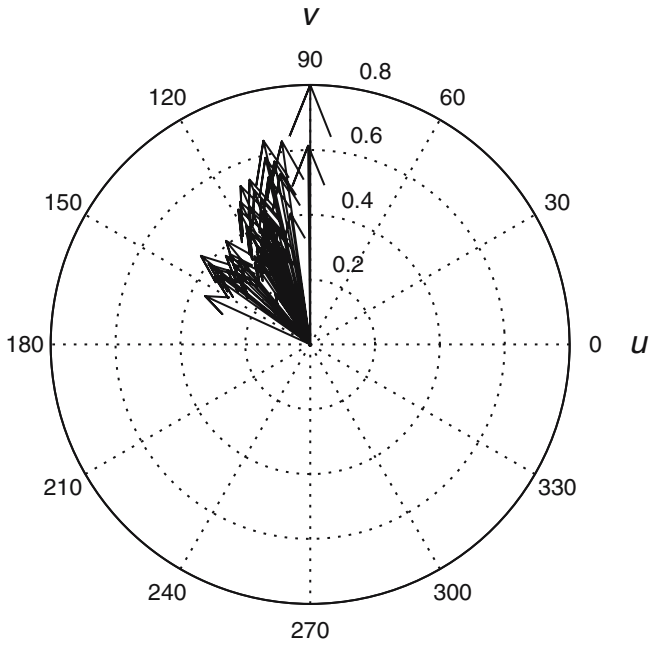

Fig. 9 Current vectors from ADCP data at z=26 m plotted every 2.5 s (when data are not flagged 'bad') from the period indicated by the *vertical bars* in the lowest panel of Fig. 8. The largest vector is just a pointer to direction 90° (v upslope current direction). Current amplitude circles are at 0.2, 0.4, 0.6 and 0.8 m s^{-1}

several hours per tidal period when dI is enhanced. These periods, clearly visible in Fig. 7b, coincide with short-term waves, more difficultly visible in v and T as enhanced 'noise'. Below, four typical examples (Fig. 7c) of these different periods will be discussed in more detail.

3.1 Upslope propagating fronts

The 5 mins detail of the passage of the upslope propagating front that is strongest in temperature drop dT/dt and largest in dI-change in the record demonstrates a clearly different time of passage in z_c, t of dI_i, i=1,..., 4 (Fig. 8). The corrected depth z_c following (5), using ψ==0, typically amounts z±2 m at mid-depth. The front in Fig. 8, extending z>60 m, shows a complex intrusion at the leading edge around z=30 m, whilst being generally well stratified (dT/dz>0). Statically unstable layers are observed just before arrival of the front, when the vertical current is strongly upward (Fig. 4) and in thin layers well after (>100 s) the frontal passage. These thin layers are alternated with layers of enhanced stratification that typically follow the passage of a front. The details in the thermistor string data are not all reproduced in the ADCP's dI data (Fig. 6), but the different arrival times of the front at the different beams are clearly visible in Fig. 8 as well as the larger-scale layers of enhanced (turbulent?) stratification that match dT/dz and dI.

The earliest arrival of the front, as observed in enhanced dI around day 114.286 is at ~15 m, first simultaneously in beams 2 and 3, followed by beam 4 just before hitting beam 1. Using (4), we compute a frontal propagation direction at this depth just east (14±10°) of upslope at a speed of c= 0.50±0.05 m s^{-1}, which is about 15% smaller than the particle speed measured at 26 m (Fig. 9). At larger distances from the bottom, the propagation direction tends to be directed slightly more to the west, whilst the currents decrease somewhat (Table 2). In general, however, $|\mathbf{u}|>c$, and both currents are more or less parallel, in upslope direction immediately after the frontal passage. Just before the front arrives, the particle speed still has a substantial alongslope (poleward) component (Fig. 4), so that within 30 s, the current veers from approximately −45 to 0° relative to upslope direction and slowly returning to −15° west of v direction (Fig. 9). The above frontal propagation direction is more or less confirmed from the different frontal appearances in the frontal beams, with a more elongated slant with increasing time and height above the bottom for beams 1, 4 and a shorter extent in time for 2, 3.

Similar observations are made for other upslope propagating fronts, although these show slightly weaker dI variations like the one in Figs. 10 and 11. Again, $|\mathbf{u}|$>c, although now $|\mathbf{u}|\approx 1.3$–$1.5c$ (Fig. 11, Table 2), whilst their directions more or less match, at least for the core of high dI variation between 10<z<40 m. A less good comparison

Table 2 Characteristics of frontal passages in Figs. 8, 9, 10, 11, 12, 13, 14 and 15, with speed (c) and direction (d) estimated using (4)

Fig.	Ref. depth (m)	Approx. time (yearday)	Sequence	c [m s^{-1}]	d (° from upslope)
8, 9	15	114.286	2, 3, 4, 1	0.50±0.05	+14±10
	45	114.286–.287	2, 3, 4, 1	0.40±0.05	−20±6
	30(back)	114.287–.288	2, 3, 4, 1	0.36±0.04	−7±10
10, 11	25(core)	114.8065	2, 3, 4, 1	0.33±0.04	−0.3±8
	25(pre-echo)	114.806	3, 2, 1, 4	0.18±0.04	+42±8
12, 13	35	114.648	4, 1, 3, 2	0.16±0.04	−164±10
14, 15	30	114.6745	4, 2, 1, 3	0.13±0.03	−83±8
	45(core)	114.675	4, 2, 3, 1	0.22±0.04	−63±10
	70(pre-echo)	114.674–.676	4, 2, 3, 1	0.14±0.03	−66±6

The 'sequence' of numbers refers to the order of passing ADCP beams 1, 2, 3 or 4 as inferred from the timing of increase in dI at a particular ref. depth (column 2)

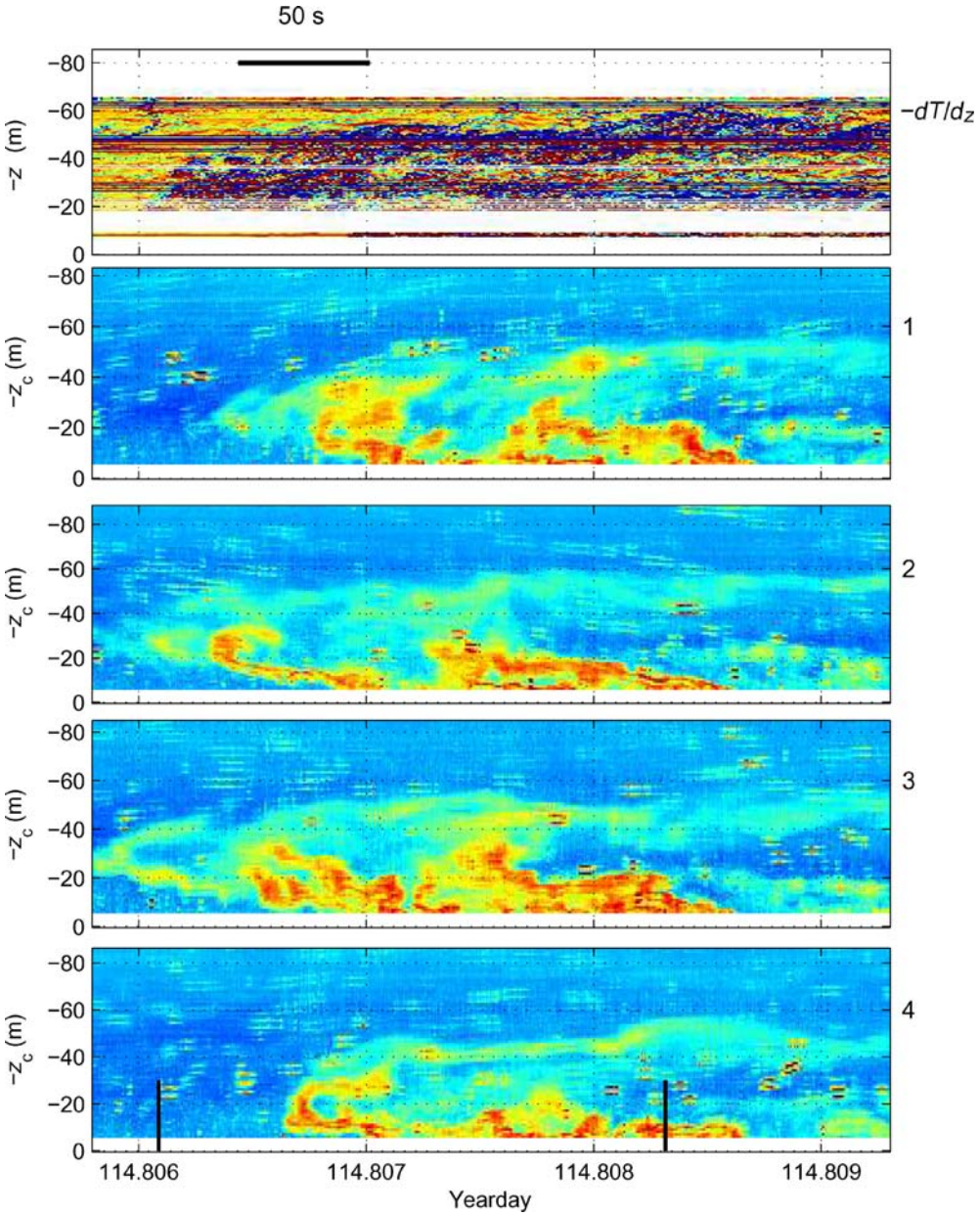

Fig. 10 As Fig. 8 with the same colour coding, but for a different upslope propagating front

between propagation and particle speed direction than above is found for the weakly enhanced *dI*, visible in green-yellow as sort of a 'pre-echo' or 'fore-shadow' around the core of high *dI*. This reflects the alongslope divergence of current just before the turbulent core (true front?) arrives, as noted in the previous example without a distinct pre-echo. The pre-echo observed here is unlikely due to unwanted side-lobe sound reflection off a curved front (of waves breaking) because the ADCP's side-lobes' sound falls off rapidly in magnitude: the 7–10 dB difference observed between the core and the 'pre-echo' would imply reflection from an angle of only ~5° off the main beam (RDI 1996). On the other hand, the different slanting of *dI* between beams 1, 4 and 2, 3 as suggested in Fig. 5 is more clearly visible in Fig. 10 than in Fig. 8, also in the shape of the pre-echo.

3.2 Downslope propagating front

Such difference in slanting in *dI* (again showing weaker variation than in Figs. 8 and 10) is even clearly visible in the example of Fig. 12, between days 114.65–114.652. In this case, beams 2, 3 show a more flat-lying, elongated layer of enhanced *dI* with time, whereas beams 1, 4 demonstrate more vertical, shorter in time layers. This points at a *dI*-front propagating more or less in downslope direction. This is confirmed from the estimates of speed and direction (Table 2) compared with particle velocities (Fig. 13). In this example, particle velocities are, on average, slightly to the west (by ~10°) of the propagation direction, whilst maximum local $|\mathbf{u}| \approx 1.5–2c$ (z~25 m). Note that for this downslope propagating front, perhaps representing a gravity current, the highest *dI* do not reach

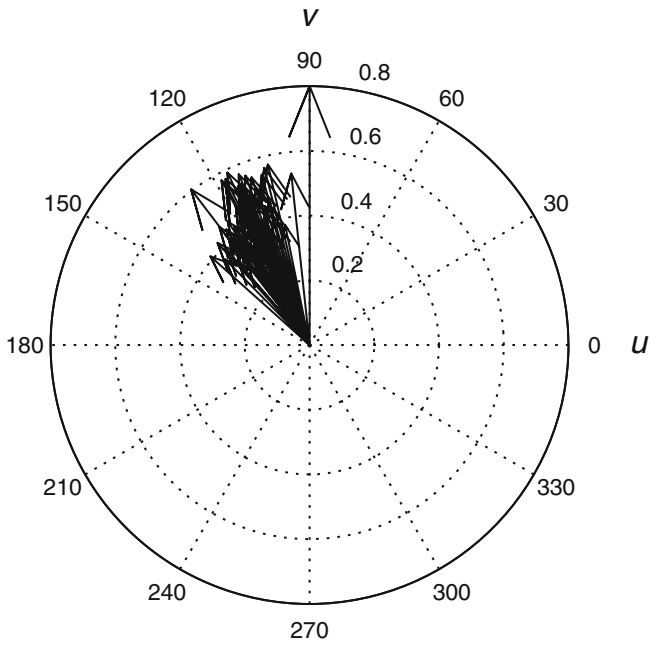

Fig. 11 As Fig. 9 but from the period indicated in the lowest panel of Fig. 10

the lowest observational level near the bottom, as in the previous examples of upslope propagating fronts.

3.3 Alongslope propagating wave

A similar ratio $|\mathbf{u}|/c>1.5$ and a *dI*-core well away from the bottom are observed for motions that do not seem to propagate related to the sloping bottom. 'Waves' propagating in alongslope direction, associated with enhanced stratification typically around $z=40$ m and well detached from enhanced near-bottom stratification for $z_c<20$ m also have propagation and particle speed direction more or less aligned to within 10° (Figs. 14 and 15; Table 2). In this example, the different slanting in z_c, t is clearly visible in the pre-echo just before the core at $z\approx45$ m around day 114.676, with now beams 1, 3 forward-up slanting and 2, 4 backward-up, with shapes more or less according to the sketch in Fig. 5c. However, except for the observation at 30 m, the order of passage is somewhat puzzling, as after 4, 2 beam 3 is hit before beam 1. This implies some turning of the wave during the passage. It may also suggest that the wave front of turbulent stratified motion is wavy itself, just like a surface waves' breaker zone at the beach.

4 Discussion

Typical dominant physical processes above sloping bottoms include non-linear solitary waves of elevation, which move on the verge of breaking ('solibores'), and oblique propagating internal waves. In the latter case, oblique waves may cause convective instabilities by deformation of the isopycnals over the slope, thereby triggering fast downslope moving bores (in the form of gravity currents), as suggested by Gemmrich and van Haren (2001). Whatever the process, the periods of elevated *dI* presented in this paper are found at all four beams within a short span of time (typically 10–30 s apart). Elevated levels in one beam are not associated with decreased levels in the opposite beam, as was found by Fuda et al. (2006). Therefore, the enhanced *dI* levels observed here are not due to flow obstruction by the bottomlander but actually evidence coherent turbulent motions.

All periods of elevated *dI* show (surprisingly) $|\mathbf{u}|>c$ and variations across the beam spread of the ADCP that are detectable over horizontal ranges of typically 10 m. On the other hand, the lesser details compared with the high-resolution thermistor string do show that the ADCP's ~4 m fully independent vertical resolution is only just about good enough to study the phenomena that prevail in sloping boundaries in the ocean. Furthermore, several problems need to be solved before a reliable *dI* means can be used easily in the future.

The raw echo intensity needs to be corrected for water attenuation and beam spreading. Somehow, general acoustic properties of attenuation in seawater (e.g. given by Urick 1975) are not precise enough if one requires determination better than ±2 dB, and the formula given by RDI (1996) does not work well for $z>20$ m. It seems better to use echo intensity in a relative manner as suggested following (3), also because different reflectors, whether material (suspended particles) or immaterial (quasi-turbulent moving stratified layers), give different elevations of echo intensity level for different transmit frequencies. As a result, the processes studied here do not just induce different *I* elevations above their (short period!) means but may also reflect different and unknown water motion and suspended particles properties. From previous studies in which independent observational means for measuring suspended particles are used (Hosegood et al. 2004), it is known that upslope moving fronts dominate sediment transport.

However, there too a quantitative relationship between suspended material and echo intensity could not be given, assumed to be due to the varying stratified turbulence and types of suspended material. Median grain sizes were observed between 150–400 μm, with a spectral sub-peak at 1,000 μm (Bonnin et al. 2006). These values are lower than the expected resonance scale of several millimetres for a 300 kHz ADCP, but uncertainty exists in the precise 'size' for acoustic reflection when particles are in suspension in a stratified turbulent environment. Here, such fronts do indeed show largest *dI* and are the only ones that extend close to the bottom, but they are observed over a very limited period of a few minutes only.

In the Hosegood et al. (2004) study, an upslope moving front was associated with $|\mathbf{u}|>c$, in fact $|\mathbf{u}|=2.1c$ was observed using arrival time differences between moorings ~2 km apart. These values do compare well with the

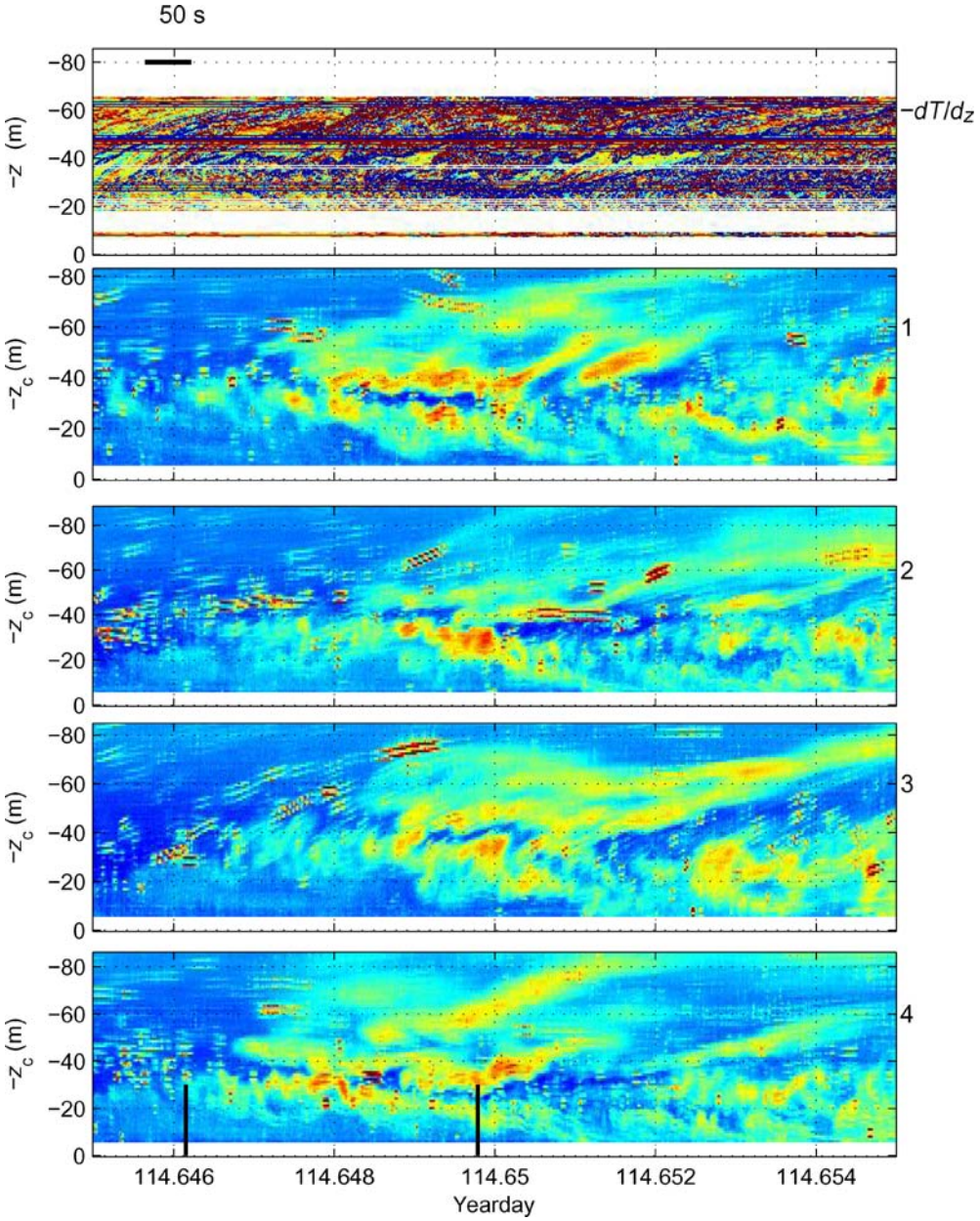

Fig. 12 As Fig. 8 but for a downslope propagating front

observations made in the present study, although this (cross-slope) distance is two orders of magnitude larger than the distance between the observing beams used here. In principle, the condition $|\mathbf{u}|>c$, understanding c as phase propagation, satisfies the kinematic instability mechanism for the overturning of a baroclinic bore (Kao et al. 1985), which conveniently explains the notion of a propagating front dominating sediment resuspension. However, one could question why all motions observed here should be overturning bores.

One problem that needs some attention is the ADCP's measurement of $|\mathbf{u}|$ during passages of such 'bores'. Clearly from the *dI*-examples given here, each passage is different at the various beams, whereas currents are averaged over the beam spread. If however, currents are confined to smaller scales than the beam spread, for example, associated with the fronts proper, every estimate made during the passage includes a correction as given for w in (6), and for u and v like (van Haren et al. 1994),

$$\begin{aligned} u &= (u_1+u_2)/2 + (w_1-w_2)\tan\theta/2, \\ v &= (v_3+v_4)/2 + (w_3-w_4)\tan\theta/2. \end{aligned} \tag{7}$$

Given the large aspect ratio $\left(|w|/|\mathbf{u}| \approx 0.25-0.5\right)$ during a frontal passage 'corrections' to true u, v involving w_i, i=1,..., 4, may be substantial (>10%), following (7).

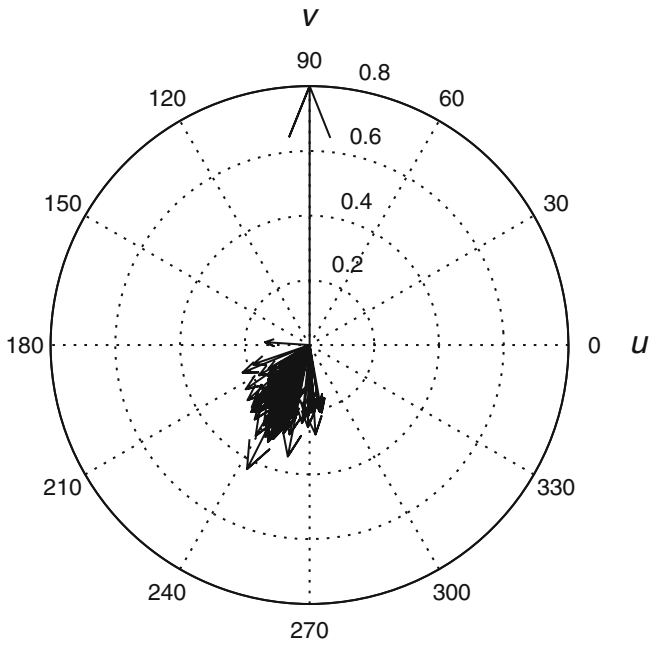

Fig. 13 As Fig. 9 but from the period indicated in the lowest panel of Fig. 12

However, these errors in estimating true u, v could work both positive and negative, depending on the direction of propagation of a bore, with respect to the orientation of the ADCP. Nevertheless, a limited comparison with independent AquaDopp currents shows a positive bias in speed (Fig. 16). Unfortunately, only the near-bottom AquaDopp could be compared with ADCP data, because at the upper AquaDopp's level of z=80 m the ADCP data were too bad.

In this example, the AquaDopp shows currents increasing up to 0.45 m s^{-1} during the frontal passage, and typically $|\mathbf{u}|$=0.40 m s^{-1}, which is close to c at day 114.287 (Table 2) and substantially (~15%) less than ADCP at $z\approx$ 16 m at that moment. During the frontal passage, ADCP data are commonly flagged bad, and w is strongly enhanced (positively). The few good current speed data are all biased higher with respect to AquaDopp's data, approximately to the amount given by the inhomogeneity terms in (7), assuming w is measured by one beam at a time only. This is not unlikely, given the different passages at the different beams following dI observations (Section 3.1, Fig. 8 for this example). However, the above AquaDopp speed is equal to $|\mathbf{u}|_{\mathrm{ADCP}}$ just before the frontal arrival at day 114.285, when w~0 (Fig. 16).

For bore-passages in the other example periods (cf. Fig. 7c), the near-bottom AquaDopp gave $|\mathbf{u}|$=0.37 m s^{-1} (114.806), 0.13 m s^{-1} (114.648) and 0.24 m s^{-1} (114.675). Similar values were observed in ADCP data at z=20–30 m just before bore arrivals (w~0). These values are all closer to the c estimates (Table 2) than the frontal $|\mathbf{u}|$ from the ADCP. Perhaps, environmental (just before bore arrival) or near-bottom particle velocities should be taken as a reference to infer the possibility of kinematic instability. As all processes identified by enhanced dI are thus associated with $|\mathbf{u}|$~c, possible errors in ADCP's currents (particle velocities) due to inhomogeneities across the beam spread seem less important, except for stress estimates for which properly determined (not flagged 'bad') current inhomogeneities do matter (van Haren et al. 1994).

The observation that propagation speeds match particle speeds, just before a front arrives, at the depth of largest turbulence velocity bears some resemblance with the propagation of a turbulent spot in a sheared flat-bottom flow (Wygnanski et al. 1976; Itsweire and Van Atta 1984). The spot is prevented from being blown apart by momentum transfer from the laminar flow to the turbulent core that thus moves slower than the undisturbed interior flow $|\mathbf{U_0}|$. Bosveld et al. (1989) demonstrate that the level of the turbulent core is found at the heights above the bottom where the spot's propagation speed matches the local particle [advection] speed: $|\mathbf{u}|$~c. These heights vary within the spot and speeds are 0.77$|\mathbf{U_0}|$ (leading edge of the spot) and 0.50$|\mathbf{U_0}|$ (trailing edge). In the present study, the turbulent core is generated via breaking waves, not by near-bottom shear instabilities. The resemblance, however, lies in the fact that the total ('turbulence' + 'background' advection) particle speed approximately equals 1.5–2c, which is close to 1/0.77–1/0.5c, at the depth of the velocity maximum and that at this depth $|\mathbf{u}|$~c when $|\mathbf{u}|$ is taken exclusively from the 'background' advection. Noting that Melville et al. (2002) estimate a turbulent core's propagation speed at 0.8 times the phase speed of a surface wave at the time of its breaking, the resemblance with a turbulent spot can be made if $|\mathbf{U_0}|$ is replaced by the wave speed.

It would have been beneficial to establish the core of highest turbulent fluxes in our deep breaking interior wave, besides levels of largest (turbulent?) excess velocities. Unfortunately, estimates of Reynolds stresses and turbulent heat fluxes using standard ADCP, originally meant for establishing internal wave induced 'large eddy' fluxes (van Haren et al. 1994), failed for the present observations. Momentum fluxes cannot be estimated using this single-ping sampling 300-kHz ADCP above a deep sloping bottom due to the large number of bad data that hamper a proper Reynolds decomposition. As such estimates also require the use of error velocity e for a proper condition of statistical homogeneity over the beam spread, even moderate ensemble averages more than, say, 10 pings do not solve much, because e is not well defined due to the large amounts of missing data in its ensembles. This contrasts with the applicability of this ADCP data analysis method in high energetic shallow water conditions where such high-sampling rate does not prevent one from

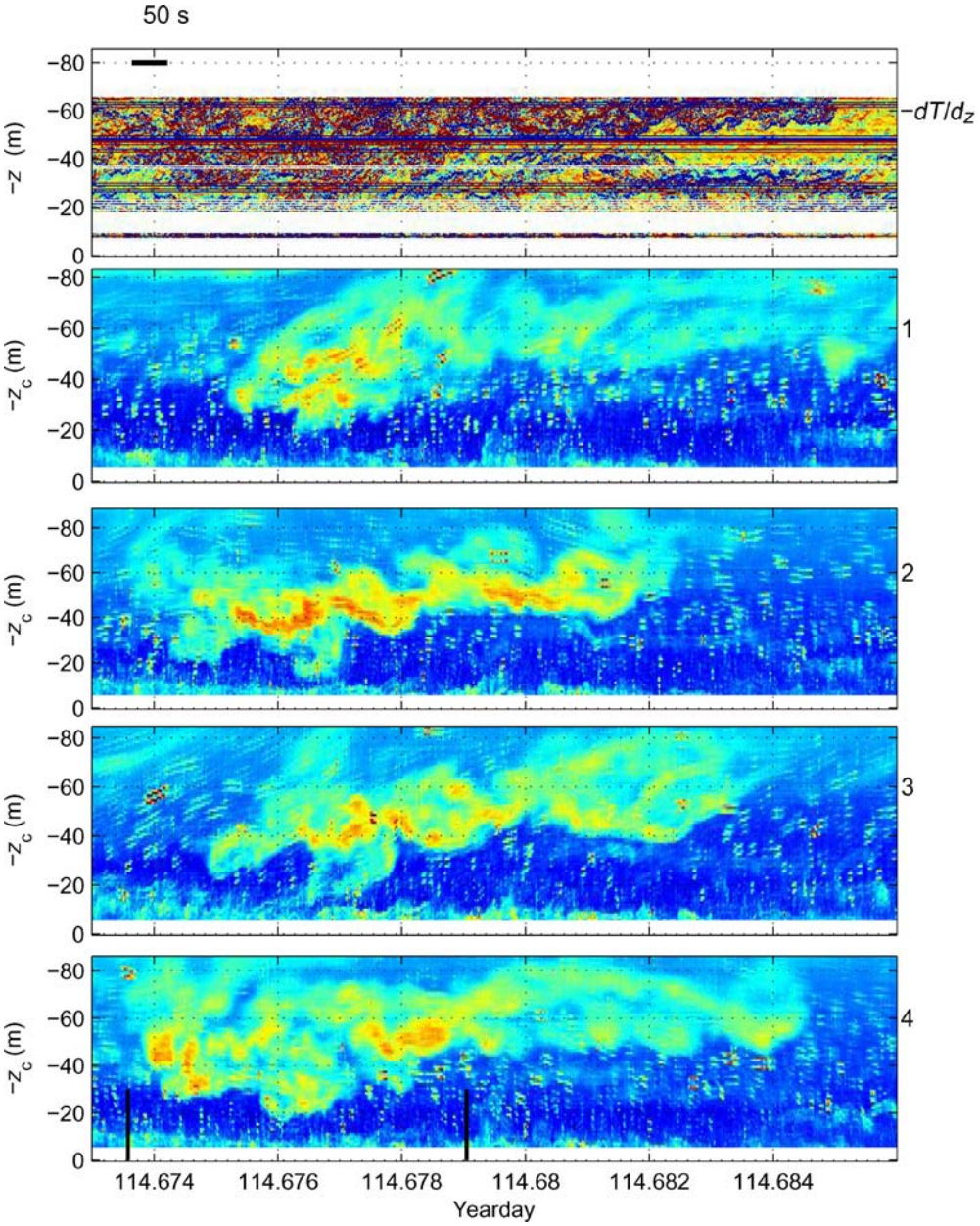

Fig. 14 As Fig. 8 but for an alongslope, poleward propagating wave

estimating fluxes in the turbulent bottom boundary layer (Lohrmann et al. 1990), except when moderate or large surface waves cause the method to breakdown also in such conditions (Souza and Howarth 2005).

5 Conclusions

Examples of high-sampling rate ADCP demonstrate the capability of using echo intensity data to identify typical processes above sloping bottoms. Shape (deformation) and propagation speed and direction can be estimated to within reasonable accuracy (<10%) via identification of the processes' passages at the different acoustic beams that are spread O(10–100 m) apart.

It is found that the propagation speed of a highly turbulent bore or wave equals the undisturbed advection (particle) speed at the depth of observation, which equals the total particle speed observed at z=1.7 m, with maximum total speeds in the turbulent core at z=20–30 m being 1.2–2 times the propagation speed. These values are observed for upslope, downslope and approximately alongslope propagating bores or waves, rendering them independent of the slope for propagation, albeit their generation seems highly associated with sloping bottoms in all cases.

Given the typical propagation speeds of 0.15–0.5 m s^{-1} observed here, the identification of these near-bottom processes requires ~1 Hz or faster sampling rate. This limits the present observational possibilities to study such processes under conditions where data return is often 'bad'.

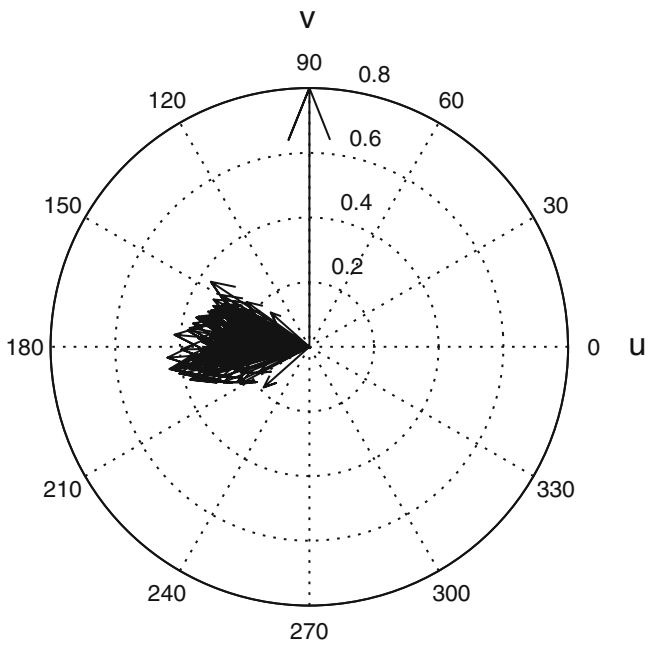

Fig. 15 As Fig. 9, but for current at z=45 m from the period indicated in the lowest panel of Fig. 14

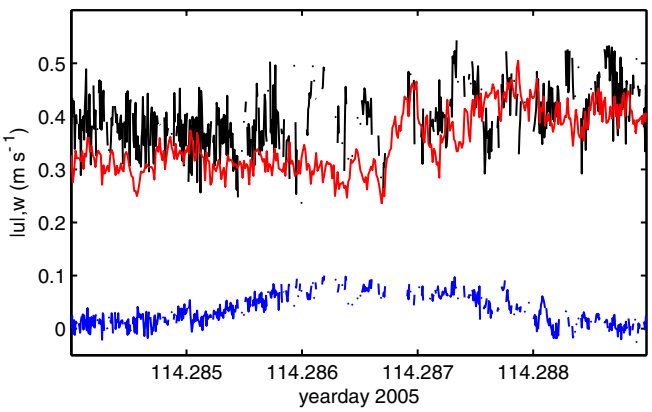

Fig. 16 Current speed just before and during frontal passage of Fig. 6 as measured by ADCP (bin 10, z≈16 m; *black*) and AquaDopp (z=1.7 m; *red*). In *blue*, w at ~16 m

For example, Reynolds stress estimates that resolve these phenomena in the high-frequency (stress) part are presently not possible.

Acknowledgement I thank the crew of the R/V Pelagia for deployment and recovery of the mooring. Theo Hillebrand and NIOZ-MTM prepared the instrumentation and moorings. Margriet Hiehle made Fig. 1.

References

Armi L (1978) Some evidence for boundary mixing in the deep ocean. J Geophys Res 83:1971–1979

Bonnin J, van Haren H, Brummer G-J, Hosegood P (2006) Burst resuspension of seabed material at the foot of the continental slope in the Rockall Channel. Mar Geol 226:167–184

Bosveld FC, van Haren JJM, Absil FGJ (1989) The measurement of <U>, <V> and <uv> inside the turbulent spot using conditionally sampled hot-wire anemometer signals. Appl Sci Res 46:291–307

Dauxois T, Didier A, Falcon E (2004) Observation of near-critical reflection of internal in a stably stratified fluid. Phys Fluids 16:1936–1941

Fuda J-L, Millot C, Hogg S, Gerber H (2006) Analysis of ADCP data above a bottom observatory. Annals Geophys 49 (in press)

Garrett C (1990) The role of secondary circulation in boundary mixing. J Geophys Res 95:3183–3189

Gemmrich JR, van Haren H (2001) Thermal fronts generated by internal waves propagating obliquely along the continental slope. J Phys Oceanogr 31:649–655

Hosegood P, van Haren H (2004) Near-bed solibores over the continental slope in the Faeroe-Shetland channel. Deep-Sea Res II 51:2943–2971

Hosegood P, Bonnin J, van Haren H (2004) Solibore-induced sediment resuspension in the Faeroe-Shetland channel. Geophys Res Lett 31:L09301. DOI 10.1029/2004GL019544

Itsweire EC, Van Atta CW (1984) An experimental investigation of coherent substructures associated with turbulent spots in a laminar boundary layer. J Fluid Mech 148:319–348

Ivey GN, Nokes RI (1989) Vertical mixing due to breaking of critical internal waves on sloping boundaries. J Fluid Mech 204:479–500

Kao TW, Pan FS, Renouard D (1985) Internal solitons on the pycnocline: generation, propagation and shoaling and breaking over a slope. J Fluid Mech 159:19–53

Klymak JM, Moum JN (2003) Internal solitary waves of elevation advancing on a shoaling shelf. Geophys Res Lett 30:2045. DOI 10.1029/2003GL017706

Lamb KG, Boegman L, Ivey G (2005) Numerical simulations of shoaling internal solitary waves in tilting tank experiments. In: Folkard A, Jones I (eds) 9th workshop on physical processes in natural waters. Lancaster University, UK, pp 21–31

Lhermitte R, Lemmin U (1990) Probing water turbulence by high frequency Doppler sonar. Geophys Res Lett 17:1549–1552

Lohrmann A, Hackett B, Røed LP (1990) High resolution measurements of turbulence, velocity and stress using a pulse-to-pulse coherent sonar. J Atmos Ocean Technol 7:19–37

MacCready P, Rhines P (1993) Slippery bottom boundary layers on a slope. J Phys Oceanogr 23:5–22

Melville WK, Veron F, White CJ (2002) The velocity field under breaking waves: coherent structures and turbulence. J Fluid Mech 454:203–233

Munk W (1966) Abyssal recipes. Deep-Sea Res 13:207–230

RDI (1996) Acoustic Doppler current profiler. Principles of operation. A practical primer. RD Instruments

Ross T, Lueck R (2003) Sound scattering from oceanic turbulence. Geophys Res Lett 30(6):1343. DOI 10.1029/2002GL016733

Souza AJ, Howarth MJ (2005) Estimates of Reynolds stress in a highly energetic shelf sea. Ocean Dyn 55:490–498

Thorpe SA (1975) The excitation, dissipation, and interaction of internal waves in the deep ocean. J Geophys Res 80:328–338

Thorpe SA, Brubaker JM (1983) Observations of sound reflection by temperature microstructure. Limnol Oceanogr 28:601–613

Urick RJ (1975) Principles of underwater sound, 2nd edn. McGraw-Hill

van Haren H (2001) Estimates of sea level, waves and winds from a bottom-mounted ADCP in a shelf sea. J Sea Res 45:1–14

van Haren H, Oakey N, Garrett C (1994) Measurements of internal wave band eddy fluxes above a sloping bottom. J Mar Res 52:909–946

van Haren H, Groenewegen R, Laan M, Koster B (2005) High sampling rate thermistor string observations at the slope of Great Meteor Seamount. Ocean Science 1:17–28, SRef-ID:1812-0792/os/2005-1-17

Vlasenko VH, Hutter K (2002) Transformation and disintegration of strongly nonlinear internal wave by topography in stratified lakes. Ann Geophys 20:2087–2103

Wygnanski I, Sokolov M, Friedman D (1976) On a turbulent 'spot' in a laminar boundary layer. J Fluid Mech 78:785–819